NUKLEONIKA 2015;60(1):23–27
doi: 10.1515/nuka-2015-0007

ORIGINAL PAPER

DE GRUYTER
OPEN

Effect of heat treatment on the shape of the hyperfine field induction distributions and magnetic properties of amorphous soft magnetic $Fe_{62}Co_{10}Y_8B_{20}$ alloy

Konrad M. Gruszka, Marcin Nabiałek, Katarzyna Błoch, Jacek Olszewski

Abstract. Thermal treatment, undertaken at just below the crystallization temperature, has led to nanocrystallization and has had a significant impact on the shape of the hyperfine field induction distributions of $Fe_{62}Co_{10}Y_8B_{20}$ alloy and on its soft magnetic properties. In the amorphous ferromagnetic alloys, it is possible to indirectly determine the effect of the structure stresses, resulting from the presence of structural defects, on the soft magnetic properties of these materials. It has been found that a change in the parameters associated with the presence of structural defects affects the shape of the hyperfine field distributions of ^{57}Fe.

Key words: bulk amorphous • Kronmüller theory • Mössbauer spectroscopy • vibrating sample magnetometer (VSM)

K. M. Gruszka✉, M. Nabiałek, K. Błoch, J. Olszewski
Institute of Physics,
Faculty of Production Engineering and Materials Technology,
Częstochowa University of Technology,
19 Armii Krajowej Ave., 42-200 Częstochowa, Poland,
Tel./Fax: +48 34 325 0795,
E-mail: kgruszka@wip.pcz.pl

Received: 18 June 2014
Accepted: 2 November 2014

Introduction

One of the main objectives of physicists and material engineers is to improve the properties of metallic alloys. For the FeSi type of alloy, commonly used in power engineering, improvement of properties is achieved through a long and fairly complicated process; this process includes: directional roll forming, annealing, and supersaturation. Despite energy-intensive efforts, textured metal sheets of FeSi are magnetostrictive alloys with reduced operating capabilities at high frequencies. During the last half-century, a group of materials called the amorphous materials has been created for electrical purposes [1, 2]. These materials are characterized by almost zero magnetostriction, low total core losses during the magnetization process, a low value of the coercive field, and high initial magnetic permeability and magnetic saturation [3]. Initially, such alloys were prepared only in the form of thin tapes, having an approximate thickness of 40 microns, which greatly limited their applications [4]. The systematic preparation of bulk amorphous alloys became possible when A. Inoue and colleagues developed three empirical criteria, described as follows. Inoue proposed that the alloy should consist of more than three components, whose radii differ by more than 12%, and also the main components of the alloy should be characterized by a negative heat mixing process [5]. Using these assumptions, amorphous material samples of thicknesses of several tens of millimeters can be produced [6, 7]. Such dimensions are already sufficient to produce magnetic cores for transformers and chokes.

The operating parameters of amorphous materials can be improved by controlled heat treatment, which leads to nanocrystallization [8, 9]. During the heating process, the migration of atoms occurs over differing distances, facilitating the growth of small grains, whilst still maintaining an amorphous matrix structure. This means that, within the alloy volume, chemical and topological ordering changes occur and interactions between matrix atoms maintain near- or medium-ranged character. One of the indirect methods for investigating the microstructure of ferromagnetic materials is the law of approach to ferromagnetic saturation in magnetization curves. These measurements provide information about the defect structure.

This paper presents the results of Mössbauer spectroscopy, X-ray diffractometry and magnetization studies. On this basis, the effect of a one-step annealing process was studied using two temperatures, both of which were below the crystallization point.

Experimental procedure

Solid amorphous samples were prepared using an injection casting process; the molten alloy was injected into a water-cooled copper mould. The resulting manufactured samples were produced in the form of plates with the following dimensions: thickness – 0.5 mm, width – 10 mm, and length – 15 mm. Then the samples were subjected to controlled annealing, which led to their nanocrystallization. Measurements of the structure were performed using a BRUKER D8 ADVANCE X-ray diffractometer. X-ray diffraction was carried out over a 2θ-angle between 30° and 120° using a measuring step of 0.02° and a measurement time per step of 5 s. The microstructure was examined using a POLON Mössbauer spectrometer, operating with a ^{57}Co source with an activity of 50 mCi. Measurements of the magnetization were performed using a LakeShore vibrating sample magnetometer: model 7301. The test samples were annealed in one step at 918 K and 928 K over a time period of 900 s. All tests were carried out on low-energy powdered samples.

Results

Figure 1 shows the X-ray diffraction pattern obtained for a sample in the as-quenched state.

The XRD pattern for the alloy in the as-quenched state has a shape that is characteristic of a sample that is in an amorphous state. There is a wide blurred maximum located within the 2θ angle of 35°–50°. This demonstrates the absence of long-range interactions. Figure 2 shows the diffraction pattern for the sample subjected to a controlled heat treatment process at a temperature of 918 K over 900 s.

As seen in Fig. 2, controlled heating of the samples resulted in the appearance of sharp, relatively intense peaks on the diffraction pattern, which correspond to four phases: Fe_5Y, α-Fe, α-FeCo, and $Fe_{23}B_6$. The positions of the peaks, derived from

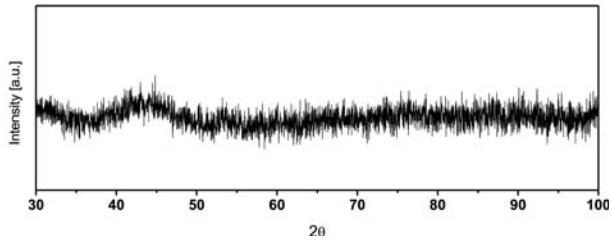

Fig. 1. X-ray diffraction pattern of $Fe_{62}Co_{10}Y_8B_{20}$ in as-quenched state.

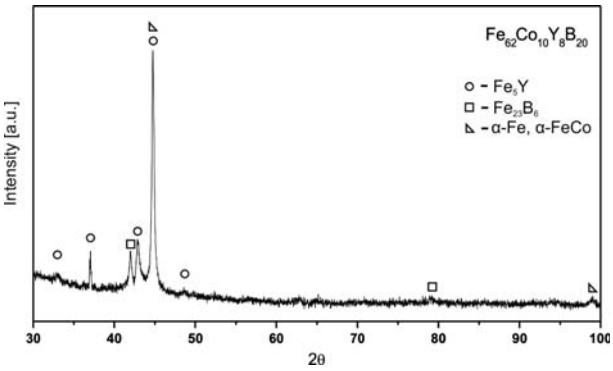

Fig. 2. X-ray diffraction pattern of $Fe_{62}Co_{10}Y_8B_{20}$ after annealing in 918 K for 900 s.

individual phases in the X-ray diffraction pattern, were in each case slightly shifted relative to the pure crystalline phases. As the stresses within the amorphous matrix are significant, and the grains are surrounded by a matrix phase, it appears that the amorphous matrix strongly affects the grain unit cells, causing their deformation. This leads to a small change in the distance of X-ray reflective surfaces. A similar situation occurred for the sample annealed at 928 K (Fig. 3).

For a sample subjected to controlled annealing at 928 K for 900 s, the same procedure to identify the crystalline phases was conducted as for the sample which had been heated to 918 K. On this basis, it was found that the same type of crystalline phases appeared in the second alloy. In contrast, the relationship between the peak intensity, derived from α-Fe phase with respect to the Fe_5Y phase, has changed. Figure 4 shows the transmission Mössbauer spectrum with the corresponding hyperfine field distribution for the sample in the as-quenched state.

The shape of the distribution of the hyperfine field, and the presence of separate low field com-

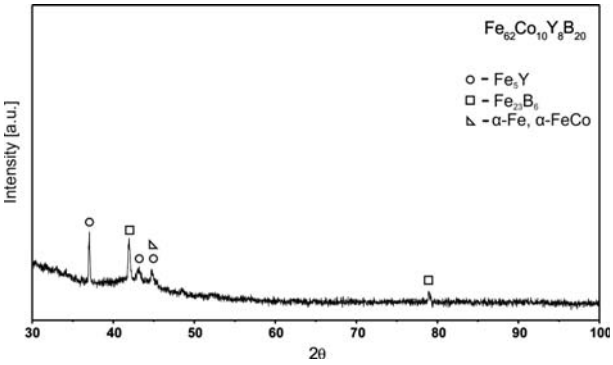

Fig. 3. X-ray diffraction pattern of $Fe_{62}Co_{10}Y_8B_{20}$ after annealing in 928 K for 900 s.

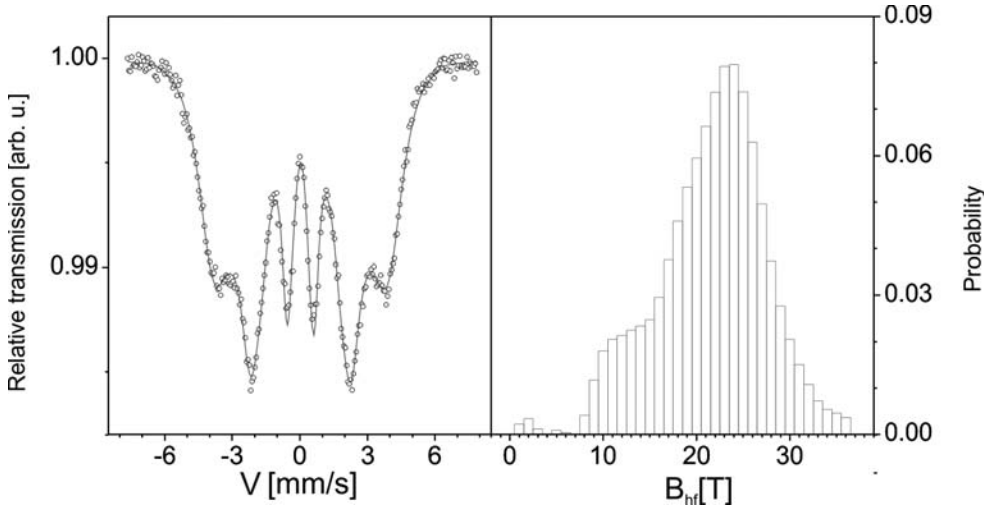

Fig. 4. Mössbauer spectrum and corresponding distribution of hyperfine field induction of $Fe_{62}Co_{10}Y_8B_{20}$ in the as-quenched state.

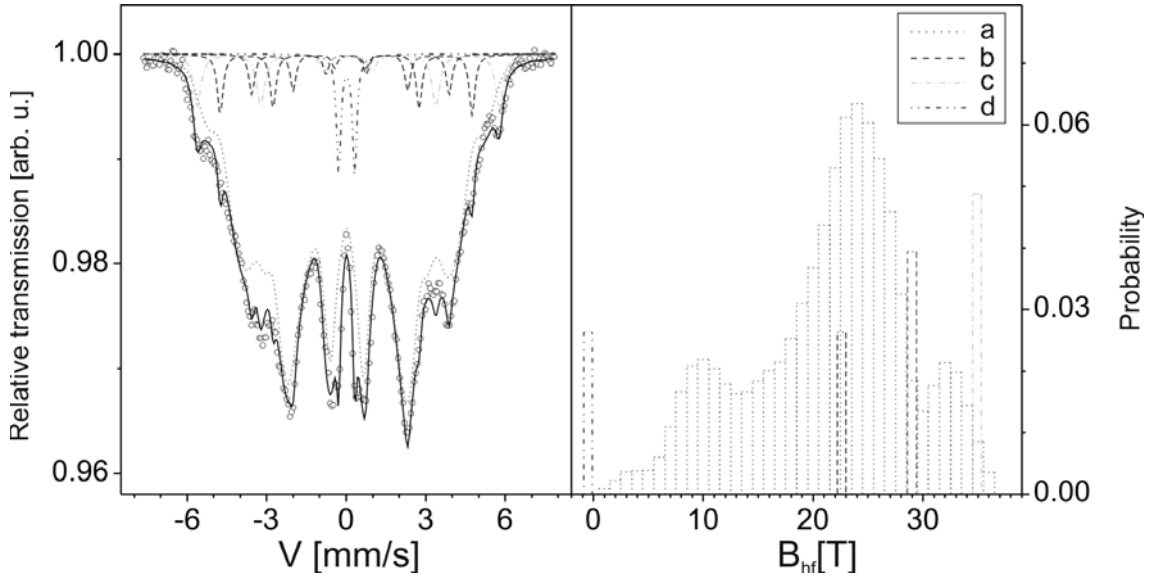

Fig. 5. Mössbauer spectrum and corresponding distribution of hyperfine field induction of $Fe_{62}Co_{10}Y_8B_{20}$ after controlled annealing in 918 K for 900 s.

ponents, indicate topological blurring of the amorphous matrix. This means that in the volume of the sample, there are several non-equilibrium ^{57}Fe neighborhoods. During the radial cooling process, a situation arises in which part of the liquid material forming the inner portion of the sample is cooled at a slightly slower speed with respect to the outer layer which is directly adjacent to the cooled mould. Figure 5 shows the Mössbauer spectrum with the corresponding hyperfine field distribution of the sample annealed at 918 K.

Controlled annealing at 918 K resulted in changes in the chemical composition of the amorphous matrix, as seen by observing the change in the hyperfine field distribution. A certain proportion of the iron atoms from the amorphous matrix had diffused, forming an α-Fe phase, leading to the depletion of its local environment. The movement of the B_{hf} field for this phase (marked as *c*) towards higher values may have been due to the incorporation of the Co atoms into its structure. The heat treatment process also caused the formation of a Fe_5Y phase, which is generally regarded as a metastable [10]. This means that the amount of this phase can vary, leading to the formation of other phases containing iron or yttrium. B_{hf} fields associated with this phase are similar to those for the $Fe_{23}B_6$ phase. The visible low field line (Fig. 5,d) on the hyperfine field distribution may indicate the occurrence of a Y rich phase. This phase is difficult to identify due to the lack of its presence in the X-ray diffraction pattern. The observed phase may be a paramagnetic phase in the three-component R-Fe-B system; most likely $Y_1Fe_4B_4$ type. Using the Rietveld refinement, the percentages of the identified crystalline phases were determined. Table 1 shows values, calculated with the assumption that the crystalline phases together make up 100%. Figure 6 shows the spectrum with the corresponding hyperfine field distribution for the sample annealed at 928 K.

The ratios of intensities associated with the phases Fe_5Y, $Fe_{23}B_6$, α-Fe and α-FeCo have changed. According to Table 1, the declining share of the α-Fe phase (marked as *c*) at the expense of $Fe_{23}B_6$ (Fig. 6,b) can

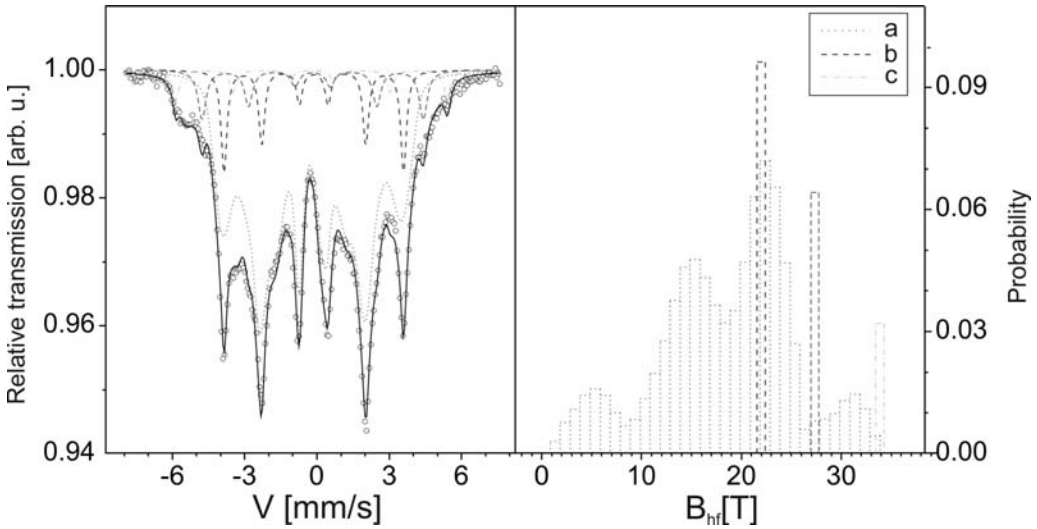

Fig. 6. Mössbauer spectrum and corresponding distribution of hyperfine field induction of $Fe_{62}Co_{10}Y_8B_{20}$ after controlled annealing in 928 K for 900 s.

Table 1. Percentage of crystalline phases

Annealing temperature [K]	Crystalline phase		
	α-Fe [%]	Fe_5Y [%]	$Fe_{23}B_6$ [%]
918	50.67	42.85	6.49
928	20.21	52.32	27.47

Table 2. Parameters obtained from the analysis of the hysteresis loops

Annealing temperature [K]	Magnetic saturation [T]	Coercive field [A/m]
–	1.27	289
918	1.19	21 070
928	1.20	1 057

be seen. The lower B_{hf} field for this phase indicates a smaller share of Co. At the same time, the hyperfine field distribution, associated with the amorphous matrix, becomes more separated, and a new mode splits. This shows the emergence of a new environmental disequilibrium near ^{57}Fe, associated with Co atoms.

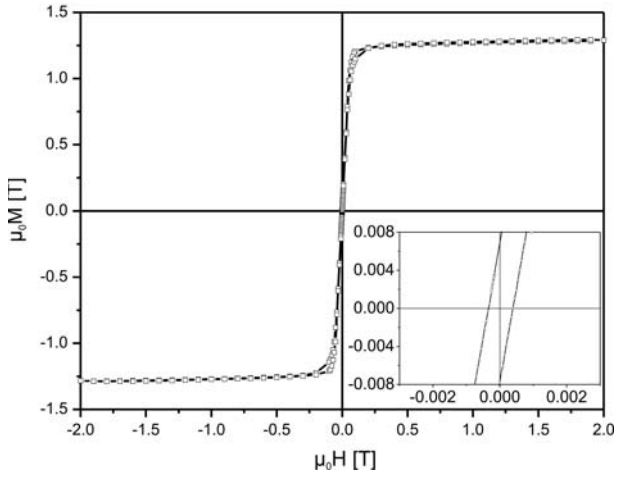

Fig. 7. Static magnetic hysteresis loop for the sample in as-quenched state.

Next, the static hysteresis loops were produced. An exemplary loop for a sample in the as-quenched state is presented in Fig. 7.

Based on the analysis of the static hysteresis loops, a set of the basic parameters is collected in Table 2. The data from Table 2 shows, that the $Fe_{62}Co_{10}Y_8B_{20}$ alloy in the amorphous state had much better H_c and $\mu_0 M_s$ parameters than after annealing. This is due to the increasing share of hard magnetic Fe_5Y and $Fe_{23}B_6$ phases and the declining share of magnetically soft α-Fe phase. Also, the appearance of Co atoms, migrating into the α-Fe phase, could be the reason for such an increase in the coercive field. On the basis of the initial magnetization curves, obtained during the registration of the static hysteresis loops, analysis was carried out in the approach to ferromagnetic saturation area. In strong fields, magnetization can be described by the following relationship [11, 12]:

$$(1)\quad \mu_0 M(H) = \mu_0 M_s \left[1 - \frac{a_{1/2}}{(\mu_0 H)^{1/2}} - \frac{a_1}{(\mu_0 H)^1} - \frac{a_2}{(\mu_0 H)^2}\right] + b(\mu_0 H)^{1/2}$$

where the first three terms are related to the presence of structural defects, and the last one describes the effect of thermally-excited spin wave damping on the magnetization in the Holstein–Primakoff process. The analysis results are summarized in Table 2. For the alloy in the state after solidification, in which there was only the amorphous phase, it was possible to determine which type of defect has the greatest impact on the magnetization process in high fields. It was found that, in the case of this sample, the process of magnetization is related to the presence of free volume conglomerates, so the relation $(a_2/(\mu_0 H)^2)$ is satisfied. These defects are sources of stresses in magnetic field strengths ranging from 0.084 T to 0.25 T.

For samples after annealing, using the calculated b parameter, it can be concluded, that the magnetization process was significantly influenced by the Holstein–Primakoff process, responsible for thermally-excited spin wave damping. This parameter is calculated from the following expression [11, 12]:

Table 3. Parameters obtained from the analysis of the initial magnetization curve. a_2 – Term responsible for presence of linear defects, b – slope of the linear fit to the damping of spin waves, D_{spf} – spin wave stiffness parameter, A_{ex} – exchange constant, l_h – exchange distance

Sample state	a_2 10^{-2} T^2	b 10^{-2} T$^{1/2}$	D_{spf} 10^{-2} meV·nm^2	A_{ex} 10^{-12} J·m^{-1}	l_h [nm]
ASQ	0.056	6.59	40.70	1.64	3.59
918 K	–	8.53	34.27	1.19	1.69
928 K	–	6.98	39.15	1.41	1.79

$$b = 3.54 g\mu_0\mu_B \left(\frac{1}{4\pi D_{spf}}\right)^{3/2} kT(g\mu_B)^{1/2} \quad (2)$$

This way, part of the external magnetic field energy is consumed to dampen spin waves, instead of the rotation of the magnetization vector, which leads to a slightly lower value of the magnetic saturation.

Conclusions

Based on the conducted studies, including XRD, Mössbauer spectroscopy, and analysis of static hysteresis loops in the approach to ferromagnetic saturation area, it can be concluded that the presence of defects in the amorphous structure (understood to be free volumes or their conglomerates) have a significant impact on the distribution of the hyperfine field. For the process of magnetization of the amorphous sample in high magnetic fields, as demonstrated using the a_2 parameter, the strongest influences are the linear defects. A high value of the spin wave stiffness (D_{spf}) and the smallest blurring of the amorphous matrix (defined as the occurrence of the minimum number of non-equilibrium neighbourhoods of ^{57}Fe), indicates an increase in the packing density of magnetic atoms. Consequently, the increase in local short-range order hinders the formation of point defects. For the sample annealed at 918 K, the calculated linear fit parameter b indicates an increase in the contribution of thermally-excited spin wave damping on the high field magnetization process. At the same time, the spin wave stiffness parameter (D_{spf}) for this sample decreases, which is associated with the occurrence of a smaller quantity of magnetic atoms in the local environment. The exchange distance (l_h) in this case is the smallest, which may suggest that pseudo-dislocation dipoles (defect conglomerates) are reduced in their linear size, or even are becoming point defects. This may indicate the diffusion of atoms in the vicinity of linear structural defects, causing their fragmentation. In the sample annealed at 928 K, another type of crystallization growth process took place, compared with samples annealed at the temperature of 918 K. A slight increase in the coercivity is due to a higher proportion of the magnetically-soft alpha-Fe phase, with respect to the semi-hard magnetic Fe_5Y and $Fe_{23}B_6$ phases. The distribution of the hyperfine field for this case demonstrates that the amorphous matrix is the most topologically fuzzy. The larger quantity of non-equilibrium positions around the close environment of ^{57}Fe and the relatively high values of the D_{spf} parameter suggest that the process of magnetization in high fields is more similar to a sample in the as-quenched state. This may indicate that the strongest impact on this process has been the occurrence of linear defects.

References

1. Linderoth, S. (2001). Synthesis and properties of amorphous and nanocrystalline alloys. Proceedings of the 22nd Riso International Symposium on Materials Science, (pp. 69–88).
2. Wang, W. H., Dong, C., & Shek, C. H. (2004). Bulk metallic glasses. *Mater. Sci. Eng.*, *44*, 45–89. DOI: 10.1016/j.mser.2004.03.001.
3. McHenry, M. E., Willard, M. A., & Laughlin, D. E. (1999). Amorphous and nanocrystalline materials for applications as soft magnets. *Prog. Mater. Sci.*, *44*, 291–433. DOI: 10.1016/S0079-6425(99)00002-X.
4. Chen, H. S., & Miller, C. E. (1970). A rapid quenching technique for the preparation of thin uniform films of amorphous solids. *Rev. Sci. Instrum.*, *41*, 1237. http://dx.doi.org/10.1063/1.1684774.
5. Inoue, A. (1998). *Bulk amorphous alloys, preparation and fundamentals characteristics*. Zurich: Trans Tech Publications.
6. Williams, P. I., Moses, A. J., Meydan, T., & Tilley, R. J. D. (2003). Amorphization of bulk magnetic materials by an arc melting technique. *J. Magn. Magn. Mater.*, *17*, 254–255. DOI: 10.1016/S0304-8853(02)00736-9.
7. Inoue, A., & Tao, Z. (1995). Fabrication of bulky Zr-based glassy alloys by suction casting into copper mold. *Mater. Trans.*, *36*(9), 1184–1187.
8. Świerczek, J. (2014). Nanocrystallization and magnetocaloric effect in amorphous Fe-Mo-Cu-B alloy. *J. Alloy. Compd.*, *615*, 255–262. DOI: 10.1016/j.jallcom.2014.06.162.
9. Pon-On, W., & Wintoai, P. (2006). Nanocrystallization in $Fe_{81}B_{13.5}Si_{3.5}C_2$ amorphous magnetic ribbons. *J. Magn. Magn. Mater.*, *320*(3/4), 81–90. DOI: 10.1016/j.jmmm.2006.04.039.
10. Maruyama, F., Nagai, H., Amako, Y., Yoshie, H., & Adahi, K. (1999). Magnetic properties of the hypothetical compound YFe_5. *Physica B*, *266*, 356–360. http://dx.doi.org/10.1016/j.physb.2012.03.050.
11. Kronmüller, H. (1979). Micromagnetism in amorphous alloys. *IEEE Trans. Magn.*, *15*, 1218–1225.
12. Kronmüller, H., & Fahnle, M. (2003). *Micromagnetism and the microstructure of ferromagnetic solids*. Cambridge University Press.